


**Transport in two-dimensional Rashba electron systems doped with interacting magnetic impurities**A. N. Zarezad and J. Abouie *Department of Physics, Institute for Advanced Studies in Basic Sciences (IASBS), Zanjan 45137-66731, Iran*

(Received 22 August 2019; revised manuscript received 6 January 2020; accepted 2 March 2020; published 12 March 2020)

We study the transport properties of two-dimensional electron systems with strong Rashba spin-orbit coupling (SOC) doped with interacting magnetic impurities. Interactions between magnetic impurities cause the formation of magnetic clusters with temperature-dependent mean sizes distributed randomly on the surface of the system. Treating magnetic clusters as scattering centers, by employing a generalized relaxation time approximation we obtain the nonequilibrium distribution functions of Rashba electrons in both regimes of above and below the band-crossing point (BCP) and present the explicit forms of the conductivity in terms of effective relaxation times. We demonstrate that the combined effects of SOC and magnetic clusters cause the system to be anisotropic and the magnetoresistance strongly depends on both the clusters' mean size and spin, the strengths of SOC, and the location of Fermi energy with respect to the BCP. Our results show that there are many contrasts between the transport properties of the system in the two regimes of above and below the BCP. By comparing the anisotropic magnetoresistance (AMR) of the two-dimensional Rashba systems with the surface AMR of three-dimensional magnetic topological insulators, we also point out the differences between these systems.

DOI: [10.1103/PhysRevB.101.115412](https://doi.org/10.1103/PhysRevB.101.115412)**I. INTRODUCTION**

Two-dimensional electron systems with Rashba spin-orbit coupling (SOC) play leading roles in novel spintronics. Locking of the spin degrees of freedom with the spatial motion of itinerant electrons splits the spin-degenerate band of the system into two parabolic bands with opposite spin-helicity intersecting each other at the band-crossing point (BCP). The presence of two bands with different spin states is one of the hallmarks of two-dimensional Rashba electron systems (2DRSs) in spintronics applications, especially in the manipulation of the spin state of electrons in the absence of external magnetic fields [1–7]. Topological changes of Fermi surface and the variations of band structure from two spin states to the valley band with a single spin state in passing through the BCP lead to several phenomena in the low-density regime [8–10], such as qualitatively significant modifications of thermoelectric and thermopower properties [10,11], modifications of the classical Dyakonov-Perel mechanism of spin relaxation [9], and the enhancement of the superconducting critical temperature in 2DRSs with strong SOC [8].

Doping of 2DRSs with magnetic impurities leads to many exotic phenomena [12–16] such as the anomalous Hall effect and anisotropic magnetoresistance (AMR). The combined effects of Rashba SOC and localized spins significantly modify the transport properties of the system; they lead to resonant enhancement of anomalous Hall conductivity [12] and giant AMR [17]. For systems with low impurity concentrations, interactions between magnetic impurities are negligible and the transport properties of the system are properly given by considering single-impurity scattering effects [17]; however

when doping increases these interactions become crucial. One of the effective solution for systems with high impurity concentrations is taking the effects of multiple scatterings into account [18]. In this paper we use the concept of magnetic clusters and study the effects of magnetic clusters on the transport properties of 2DRSs. Exchange interactions between magnetic impurities cause the formation of clusters where they are constructed of correlated magnetic impurities fluctuating consistently in the same direction. The clusters' mean sizes (CMSs) and their number (CN) depend on temperature. The cluster model was first proposed in Refs. [19,20] for explaining the temperature dependence of the magnetoresistance of magnetic semiconductors, and recently developed for investigating the surface conductivity of three-dimensional magnetic topological insulators [21]. In this paper by treating magnetic clusters as scattering centers randomly distributed on the surface of the 2DRSs, and considering a long-range scattering potential, we demonstrate that the combined effects of Rashba SOC and magnetic clusters cause the system to be anisotropic and the anisotropy strongly depends on different parameters such as the clusters' mean size and spin direction, the strengths of SOC, and the locations of Fermi energy with respect to the BCP. We obtain the nonequilibrium distribution functions of electrons in different bands within the semiclassical Boltzmann approach, and compute the conductivity and the AMR of the system in both regimes of above and below the BCP. We demonstrate that for large CMSs the angular dependence of the AMR is unconventional in comparison with conventional ferromagnets. We also show that there are many contrasts between the transport properties of the system in the two regimes of above and below the BCP.

This paper is organized as follows. In Sec. II, we obtain the band structure of 2DRSs and present the generalized relaxation time approximation (GRTA) in order to find the

\*jahan@iasbs.ac.ir

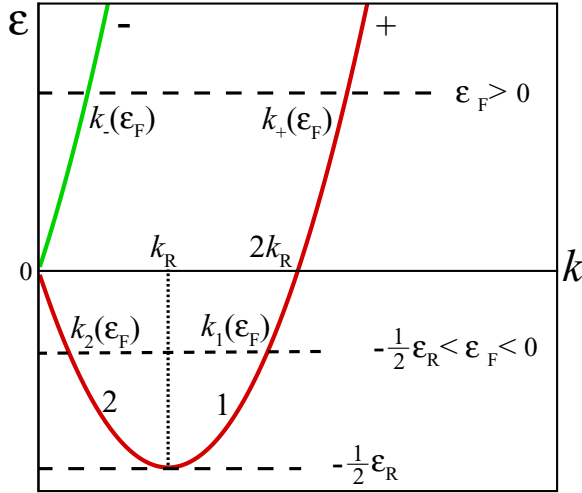


FIG. 1. The band structure of the 2DRS. Above the BCP ( $\varepsilon_F > 0$ ) Fermi energy intersects the band  $n$ , at the point  $k_n(\varepsilon_F) = k_F^0(n\sqrt{\varepsilon_R} + \sqrt{1 + \varepsilon_R})$ . However, when the Fermi energy lies in the interval  $-\frac{\varepsilon_R}{2} < \varepsilon_F < 0$ , it intersects the branch  $\nu$  at the point  $k_\nu(\varepsilon_F) = k_F^0[\sqrt{\varepsilon_R} - (-1)^\nu \sqrt{\varepsilon_R - 1}]$ . The parameter  $k_F^0 = \sqrt{2m\varepsilon_F/\hbar^2}$  is the Fermi wave number of free electrons (without SOC).  $\varepsilon_R$  is defined as  $\varepsilon_R/2\varepsilon_F$  for  $\varepsilon_F > 0$ , and  $\varepsilon_R/(2|\varepsilon_F|)$  for  $\varepsilon_F < 0$ .

nonequilibrium distribution functions of electrons in each bands. In Sec. III, we present the explicit form of the conductivities in the two-band regime. In this section we also compare the relaxation times obtained by other approaches. The results of the single-band regime are presented in Sec. IV. The summaries and conclusions are given in Sec. V. At the end of this paper we present the details of our calculations in three different Appendices.

## II. SCATTERING POTENTIAL AND GRTA

The Hamiltonian of a 2DRS is given by

$$H_0 = \frac{\hbar^2 k^2}{2m} + \alpha(\sigma_y k_x - \sigma_x k_y), \quad (1)$$

where the first term is the kinetic energy of electrons with effective mass  $m$ , and the second term is the Rashba SOC with the strength of  $\alpha$ . The Pauli matrices  $\sigma_{x,y}$  indicate spin of electrons, and  $k_{x,y}$  are the two components of the electrons' wave vector,  $\mathbf{k}$ . The eigenenergies and eigenstates of the Hamiltonian  $H_0$  are given by

$$\varepsilon_n(k) = \frac{\hbar^2 k^2}{2m} - nk\alpha = \frac{\hbar^2}{2m}(k - nk_R)^2 - \frac{\varepsilon_R}{2}, \quad (2)$$

$$\psi_n(\mathbf{k}, \mathbf{r}) = \frac{e^{i\mathbf{k}\cdot\mathbf{r}}}{\sqrt{2A}} \begin{pmatrix} -nie^{-i\phi} \\ 1 \end{pmatrix}, \quad (3)$$

where  $n$  ( $= \pm$ ) represents the Rashba bands,  $\varepsilon_R = \frac{m\alpha^2}{\hbar^2}$  is the Rashba energy ( $\varepsilon_R/2$  is the minimum value of the band  $+$  at  $k_R = \frac{m\alpha}{\hbar^2}$ ),  $A$  is the area of the 2DRS, and  $\phi = \arctan(k_y/k_x)$  is the polar angle of the  $\mathbf{k}$  vector. In the presence of SOC, the energy spectrum splits into two energy bands  $+$  and  $-$ , intersecting each other at the band-crossing point (BCP), illustrated in Fig. 1.

Strong SOC has been observed in several materials [22–25], such as the Te-terminated surface of the polar semiconductor BiTeX ( $X=I, \text{Br}, \text{and Cl}$ ) [26–31], where Rashba SOC is on the order of 1.7–3.8 eVÅ, which is one order of magnitude larger than the Rashba SOC in conventional III-V semiconductor heterostructures.

Above the BCP, band velocities are readily obtained as  $\mathbf{v}_\pm = \frac{\hbar}{m}(N_0/N_\pm)\mathbf{k}_\pm$ , where  $N_\pm(\varepsilon)$ , the density of states (DOS) in the bands  $\pm$ , is given by

$$N_\pm(\varepsilon) = N_0 \frac{k_\pm(\varepsilon)}{k_\pm(\varepsilon) - nk_R}. \quad (4)$$

Here,  $N_0 = \frac{m}{2\pi\hbar^2}$  is the DOS of 2D free electron systems. Above the BCP, band velocities are always in the direction of the  $\mathbf{k}$  vector. Below the BCP, the energy  $+$  behaves non-monotonically: it decreases by increasing  $k$  for  $k < k_R$  (branch 2), becomes minimum at  $k_R$ , and increases by  $k$  for  $k > k_R$  (branch 1). The band velocities for the two branches 1 and 2 are given by  $\mathbf{v}_\nu = (-1)^\nu \frac{\hbar}{m}(N_0/N_\nu)\mathbf{k}_\nu$ , where the DOS  $N_\nu(\varepsilon)$  is given by

$$N_\nu(\varepsilon) = N_0 \frac{k_\nu(\varepsilon)}{|k_\nu(\varepsilon) - k_R|}. \quad (5)$$

In a two-dimensional electron system doped with magnetic impurities, the interaction between an electron with spin  $\sigma$  at the position  $\mathbf{r}$ , with an impurity with spin  $\mathbf{S}$  located at  $\mathbf{R}$ , is given by the following Hamiltonian:

$$H_{\sigma S} = -J(\mathbf{r} - \mathbf{R})\sigma(\mathbf{r}) \cdot \mathbf{S}(\mathbf{R}), \quad (6)$$

where  $J(\mathbf{r} - \mathbf{R})$  is the exchange coupling. In dilute magnetic systems itinerant electrons interact with individual single magnetic impurities, and the exchange coupling is modeled by the Dirac  $\delta$  function as  $J(\mathbf{r} - \mathbf{R}) \propto J_0\delta(\mathbf{r} - \mathbf{R})$ , where  $J_0$  is a coupling constant on the order of a few meV [32–34]. When doping of magnetic impurities increases, the interactions between magnetic impurities become significant and we should consider their effects on the transport properties of the system. Actually, the exchange interactions between impurities lead to the formation of various magnetic domains with different sizes in the entire system. These ordered domains, which are called “magnetic clusters,” are constructed of correlated magnetic impurities with the same spin directions. Scattering of electrons by these clusters (rather than single impurities) alters the transport properties of the system [21]. In order to investigate the effects of magnetic clusters on the conductivity, we model the scattering potential of electrons by clusters as

$$H_{\sigma S} = J_0 \exp(-|\mathbf{r} - \mathbf{R}|/\xi)\sigma(\mathbf{r}) \cdot \mathbf{S}(\mathbf{R}), \quad (7)$$

where  $\xi$  is the clusters' mean size, depending on both temperature and impurity-impurity exchange coupling, and  $\sigma$  is the spin of the magnetic cluster located at  $\mathbf{R}$ . The scattering potential in Eq. (7) is long-range and  $\xi$  appears as a characteristic length, indicating the range of scattering potential. Without loss of generality, we consider the spins of clusters as classical vectors in the  $yz$  plane, i.e.,  $\mathbf{S} = S(0, \sin\theta, \cos\theta)$ , where  $\theta$  is the tilt angle of  $\mathbf{S}$  with the axis normal to the surface of the 2DRS (see Fig. 2).

In order to obtain the nonequilibrium distribution function of electrons in the presence of magnetic clusters, we use the semiclassical Boltzmann approach. In the presence of

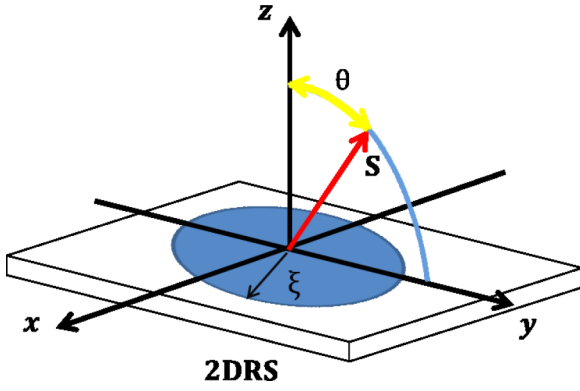


FIG. 2. The schematic illustration of a single magnetic cluster with size of  $\xi$ , centered at  $\mathbf{R} = 0$ . Red arrow represents cluster's spin  $\mathbf{S}$ , and  $\theta$  is the tilt angle of  $\mathbf{S}$  with the  $z$  axis.  $\mathbf{S}$  is subjected to rotation in the  $zy$  plane.

a uniform electric field  $\mathbf{E}$ , the nonequilibrium distribution function of electrons in the band  $n$ ,  $f_n(\mathbf{k}, \mathbf{E})$ , satisfies the following relation:

$$\left(\frac{\partial f_n}{\partial t}\right)_{\text{coll}} = e\mathbf{v}_n(\mathbf{k}) \cdot \mathbf{E} \left(\frac{\partial f_n^0}{\partial \varepsilon_n}\right), \quad (8)$$

where  $\mathbf{v}_n(\mathbf{k})$  is the band velocity, and  $f_n^0$  is the Fermi-Dirac distribution function in the band  $n$ . By considering elastic scatterings and using detailed balance, the left-hand side of Eq. (8) is also written as [35]

$$\begin{aligned} \left(\frac{\partial f_n}{\partial t}\right)_{\text{coll}} = & \sum_{n', \mathbf{k}'} w_{n, n'}(\mathbf{k}, \mathbf{k}') [1 - f_n(\mathbf{k})] f_{n'}(\mathbf{k}') \\ & - \sum_{n', \mathbf{k}'} w_{n', n}(\mathbf{k}', \mathbf{k}) [1 - f_{n'}(\mathbf{k}')] f_n(\mathbf{k}), \end{aligned} \quad (9)$$

where  $w_{n, n'}(\mathbf{k}, \mathbf{k}')$  is the transition rate between the two eigenstates of the Hamiltonian  $H_0(|n\mathbf{k}\rangle$  and  $|n'\mathbf{k}'\rangle$ ). Using Eqs. (8) and (9), the Boltzmann equation is written as

$$e\mathbf{v}_n(\mathbf{k}) \cdot \mathbf{E} \left(\frac{\partial f_n^0}{\partial \varepsilon_n}\right) = \sum_{n', \mathbf{k}'} w_{n, n'}(\mathbf{k}, \mathbf{k}') [f_{n'}(\mathbf{k}') - f_n(\mathbf{k})], \quad (10)$$

where the interaction between electrons has been neglected.

In the isotropic 2DRSs ( $\theta = 0$ ), the scattering rate depends on the angle between  $\mathbf{k}$  and  $\mathbf{k}'$  ( $\Delta\phi = \phi - \phi'$ ), and relaxation times of electrons in the bands  $+$  and  $-$  depend only on the magnitudes of  $\mathbf{k}$  and  $\mathbf{k}'$ . By using standard methods such as the modified relaxation time approximation (MRTA) [17,36] and other analytical exact solutions of self-consistent equations for relaxation times [11,37], we can solve Eq. (10). But in the anisotropic case, when  $\theta \neq 0$ , the scattering rates as well as the relaxation times depend on both the magnitudes and the directions of  $\mathbf{k}$  and  $\mathbf{k}'$ , so it is no longer possible to use the standard methods for obtaining the nonequilibrium distribution function  $f_n$ . Using the method developed by Vybrony *et al.* [17], we approximate  $f_n$  as

$$f_n - f_n^0 = eE v_n(\mathbf{k}) \left(\frac{\partial f_n^0}{\partial \varepsilon_n}\right) [a_n(\Phi) \cos \chi + b_n(\Phi) \sin \chi], \quad (11)$$

where  $\Phi$  is the polar angle of the band velocity  $\mathbf{v}_n$ , and  $\chi$  is the angle between the electric field and  $x$  axis.

Above the BCP, band velocities are always in the direction of the  $\mathbf{k}$  vector and the polar angle  $\Phi$  is equal to  $\phi$ . Below the BCP, in branch 1, the band velocity  $\mathbf{v}_1$  and the  $\mathbf{k}$  vector are parallel and  $\Phi = \phi$ . For this branch we will write the nonequilibrium distribution function the same as the two-band case. However, in branch 2 the band velocity  $\mathbf{v}_2$  is antiparallel with  $\mathbf{k}$ , and  $\Phi = -\phi$ . The distribution functions of electrons in this branch will be expressed in terms of the polar angle of the  $\mathbf{k}$  vector, with some modifications.

In the following we investigate the transport properties of the 2DRSs, for the two regimes of  $\varepsilon_F > 0$  and  $\varepsilon_F < 0$ , in the two separate sections.

### III. TWO-BAND SCATTERING ( $\varepsilon_F > 0$ )

The conductivity of electron systems is obtained from the following general formula:

$$\sigma_{ij} = \frac{-e}{E_j} \sum_n \int \frac{d^2k}{(2\pi)^2} v_n^i(\mathbf{k}) f_n(\mathbf{k}, \mathbf{E}), \quad (12)$$

where  $i$  and  $j$  denote the  $x$  and  $y$  directions, and  $v_n^i(\mathbf{k})$  is the band velocity along the  $i$  direction. Above the BCP the band velocity is given by  $\mathbf{v}_n(\mathbf{k}) = v_n(k)(\cos \phi, \sin \phi)$  and the conductivities in the  $x$  and  $y$  directions are obtained as (see Appendix A)

$$\begin{aligned} \sigma_{xx} &= \frac{e^2}{4\pi} \int k dk \sum_{n=\pm} \left[ v_n^2(k) \left(-\frac{\partial f_n^0}{\partial \varepsilon_n}\right) c_1^n(k) \right], \\ \sigma_{yy} &= \frac{e^2}{4\pi} \int k dk \sum_{n=\pm} \left[ v_n^2(k) \left(-\frac{\partial f_n^0}{\partial \varepsilon_n}\right) s_1^n(k) \right], \end{aligned} \quad (13)$$

where the coefficients  $c_1^\pm(k)$  and  $s_1^\pm(k)$  are introduced in Appendix A. They have a dimension of time and depend on the parameters  $k$ ,  $\theta$ ,  $\xi$ , and  $\alpha$ . We treat them as momentum relaxation times of electrons along the  $x$  and  $y$  directions and define the following dimensionless variables:  $\tau_x^\pm = \omega_0 c_1^\pm$  and  $\tau_y^\pm = \omega_0 s_1^\pm$ , where  $\omega_0 = \frac{\pi \hbar n_c J_0^2 S^2}{4A m \varepsilon_F}$  is a scale factor with units of the scattering rate.

Since the temperature region where  $\xi$  and  $\eta_c$  vary is much smaller than the Fermi temperature of the system, we can approximate the function  $\partial f_n^0 / \partial \varepsilon_n$  with the Dirac delta function  $\delta(\varepsilon - \varepsilon_F)$ . For example the Curie temperature for the ferromagnetic IV-VI compounds like  $\text{Ge}_{1-x}\text{Mn}_x\text{Te}$  is about 80 K [38]. Moreover, in a large class of materials containing heavy  $5d$  elements together with rare-earth or transition metal elements, the critical temperature is much lower than the Fermi temperature. These materials are nonmagnetic in the bulk but exhibit 2D magnetism at the surface. For example  $\text{EuIr}_2\text{Si}_2$  with nonmagnetic bulk reveals controllable 2D ferromagnetism below 48 K [39].

With the above assumptions, the conductivities (13) reduce to

$$\begin{aligned} \sigma_{xx} &= \sigma_0 \sqrt{\tilde{\varepsilon}_R + 1} \sum_{n=\pm} \tau_x^n(\varepsilon_F) [n\sqrt{\tilde{\varepsilon}_R} + \sqrt{\tilde{\varepsilon}_R + 1}], \\ \sigma_{yy} &= \sigma_0 \sqrt{\tilde{\varepsilon}_R + 1} \sum_{n=\pm} \tau_y^n(\varepsilon_F) [n\sqrt{\tilde{\varepsilon}_R} + \sqrt{\tilde{\varepsilon}_R + 1}], \end{aligned} \quad (14)$$

where  $\sigma_0 = \left(\frac{e^2}{2h}\right) \frac{8mA\xi^3}{\pi\eta_c J_0^2 S^2 \hbar^2}$  is the conductivity of the system in the absence of SOC when  $\xi$  is about the Fermi wavelength of free electrons  $\lambda_F^0 = h/\sqrt{2m\varepsilon_F}$ .  $\eta_c$  is the number of clusters (CN) with mean size. In general, both  $\xi$  and  $\eta_c$  depend on temperature. They are not independent and we should take into account the dependence of  $\eta_c$  to  $\xi$  on the conductivity. However, according to the function of  $\eta_c(\xi)$  considering this dependence does not change the behavior of the conductivity, qualitatively, and one can consider the number of clusters  $\eta_c$  as a scale factor in the conductivity.

When the spins of magnetic clusters are normal to the surface of the 2DRS ( $\theta = 0$ ), the scattering amplitude depends only on  $\Delta\phi$  and the system is isotropic. In this case, the coefficients matrix in Eq. (A7) reduces to a block-diagonal matrix and the relaxation times  $\tau_x = (\tau_x^+, \tau_x^-)$  and  $\tau_y = (\tau_y^+, \tau_y^-)$  are simplified to

$$\tau_x = \tau_y = \tau = \mathbf{A}_0^{-1} \cdot \mathbf{d}_1, \quad (15)$$

where  $\tau = (\tau^+, \tau^-)$ .

We have plotted in Fig. 3 the relaxation times  $\tau^\pm$  versus CMS, for different strengths of SOC. As is seen they decrease by increasing  $\tilde{\xi}$ , become minimum, and gradually go to infinity at large CMSs. The emergence of such a minimum (which is a combined effect of SOC and magnetic clusters) is attributed to the efficient scattering of electrons when their Fermi wavelength is comparable with CMS. At a given Fermi energy, the Fermi wavelength of electrons in the band  $n$  depends on the strength of SOC as  $\lambda_F^n = \lambda_F^0 / (\sqrt{\tilde{\varepsilon}_R + 1} + n\sqrt{\tilde{\varepsilon}_R})$ . When CMS increases, maximum scattering of electrons in the band  $n$  occurs at  $\lambda_F^n \sim 2\pi\xi$ . Since  $\lambda_F^+ \neq \lambda_F^-$ , minimums of  $\tau^\pm$  appear at different CMSs. For small SOC the Fermi wavelength  $\lambda_F^n$  behaves as  $\lambda_F^n \sim \lambda_F^0(1 - n\sqrt{\tilde{\varepsilon}_R})$ , and the separation between minimums increases by SOC as  $\sqrt{\tilde{\varepsilon}_R}$ . For large SOC the minimum of  $\tau^+$  gradually approaches the point  $\tilde{\xi} = 0$ , but  $\tau^-$  becomes minimum at larger CMSs. Also, since  $\lambda_F^+$  is smaller than  $\lambda_F^-$ , the relaxation time  $\tau^+$  is always larger than  $\tau^-$ .

In the isotropic case the relaxation times  $\tau_x^n$  and  $\tau_y^n$  and consequently the conductivities along the  $x$  and  $y$  directions are equal ( $\sigma_{xx} = \sigma_{yy} = \sigma$ ). We have plotted in Fig. 4 the conductivity  $\sigma$  versus CMS, for different strengths of SOC. For small CMSs the conductivity is very large; however by increasing CMS it decreases rapidly, becomes minimum at a  $\tilde{\xi}$  (say  $\tilde{\xi}_{\min}$ ), and finally increases monotonically, as shown in Fig. 4. To describe this nonmonotonic behavior, we investigate the behavior of the scattering amplitude. Let us write the  $T$  matrix as

$$T_{\mathbf{k},\mathbf{k}'}^{n,n'} = T_{n,n'}^\theta T_{\mathbf{k},\mathbf{k}'}^\xi, \quad (16)$$

which is a multiple of two parts: (1) The spin-dependent part,  $T_{n,n'}^\theta$ , which depends on the tilt angle  $\theta$ . This part is given by

$$T_{n,n'}^\theta = \cos\theta(nm'e^{i\Delta\phi} - 1) - \sin\theta(n'e^{-i\phi'} + ne^{i\phi}). \quad (17)$$

(2) The  $\xi$ -dependent part, written as

$$T_{\mathbf{k},\mathbf{k}'}^\xi = \int d\mathbf{r} e^{-i\mathbf{k}\cdot\mathbf{r}} e^{-r/\xi} e^{i\mathbf{k}'\cdot\mathbf{r}}, \quad (18)$$

which depends on the clusters' mean size,  $\xi$ .

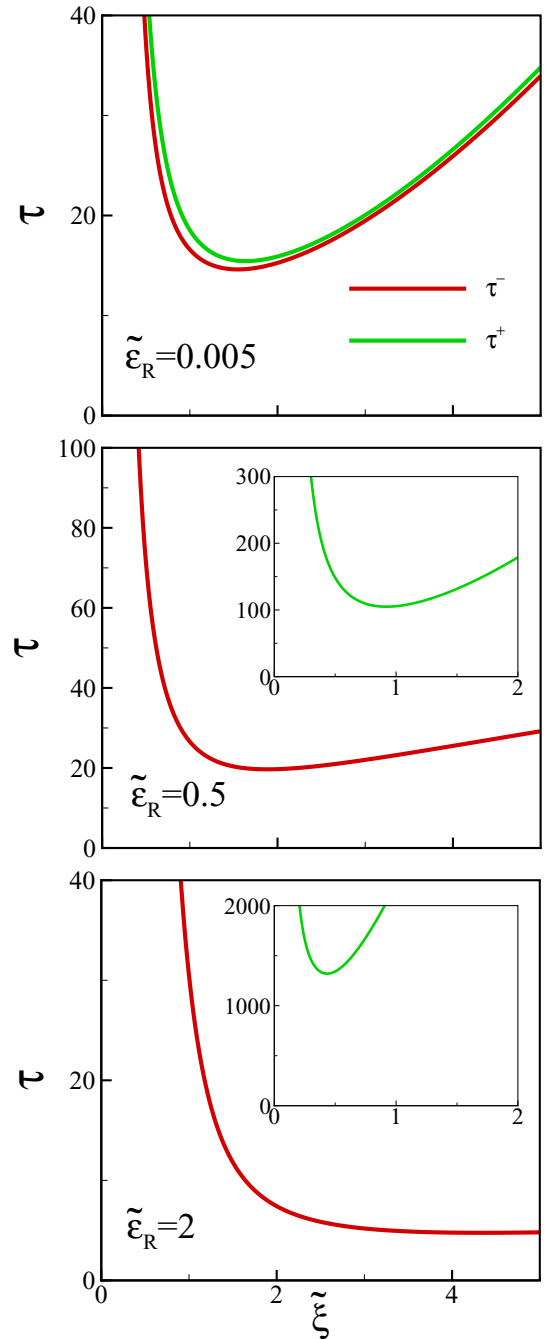


FIG. 3. The relaxation times of electrons in the bands + and - vs  $\tilde{\xi} = \xi\sqrt{2m\varepsilon_F}/\hbar^2$ , for different strengths of SOC, when the spins of magnetic clusters are normal to the surface of the 2DRS ( $\theta = 0$ ). Here, Fermi energy is located above the BCP.

For large CMSs, in the limit of  $\xi \rightarrow \infty$ , the  $\xi$ -dependent part of the  $T$  matrix becomes proportional to the Dirac delta function  $\delta(\mathbf{k} - \mathbf{k}')$ , and consequently only intraband forward scatterings have determinant effects on the  $T$  matrix. On the other hand, from the spin-dependent part we see that at  $\theta = 0$ , the intraband scattering amplitudes,  $T_{+,+}^\theta$  and  $T_{-,-}^\theta$ , are equal to  $\exp(i\Delta\phi) - 1$ . These amplitudes are vanishing for  $\Delta\phi = 0$ , which means that no intraband forward scattering occurs in the system. Summing up the above arguments, we conclude

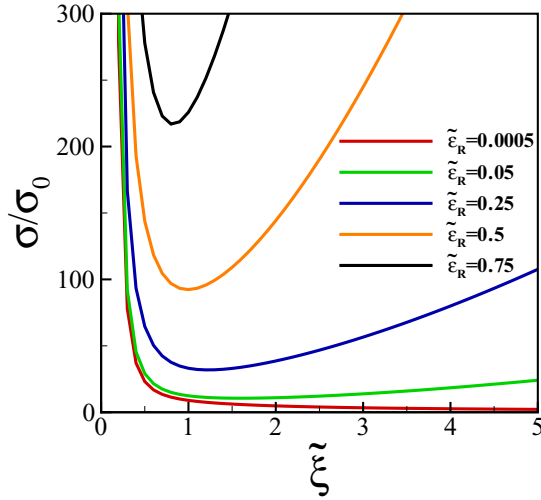


FIG. 4. The conductivity of the isotropic 2DRS ( $\theta = 0$ ) vs CMS for different strengths of SOC. At a given Fermi energy above the BCP ( $\varepsilon_F > 0$ ), by increasing the strength of SOC, the conductivity increases and its minimum emerges at smaller values of  $\xi$ .

that at  $\theta = 0$ , for  $\xi \rightarrow \infty$  the scattering amplitude approaches zero which results in an infinite conductivity.

For small CMSs, in the limit of  $\xi \rightarrow 0$ , the scattering potential becomes weaker, and thus no scattering happens in the system and the conductivity is very large.

We can also explain the physics behind the nonmonotonic behavior of the conductivity by comparing the CMS,  $\xi$ , with the average Fermi wavelength of electrons. This wavelength is readily obtained as

$$\lambda_F^{av} = \frac{N_+}{N_+ + N_-} \lambda_F^+ + \frac{N_-}{N_+ + N_-} \lambda_F^- = \frac{\lambda_F^0}{\sqrt{1 + \tilde{\varepsilon}_R}}. \quad (19)$$

At a given  $\tilde{\varepsilon}_R$ , when CMS increases, backscattering of electrons by clusters increases until  $\xi$  becomes comparable with  $\lambda_F^{av}$ . When  $\xi \sim \lambda_F^{av}/2\pi$  the ability of clusters to scatter electrons is greatly increased and electrons are most efficiently scattered by magnetic clusters. At this point the conductivity becomes minimum. But for CMSs larger than  $\lambda_F^{av}$ , this ability decreases and the conductivity enhances monotonically by increasing CMS.

The location of the minimum of the conductivity depends on the strength of SOC. In the absence of SOC, the Rashba system (1) reduces to a free electron system and the conductivity always decreases by increasing  $\xi$ . However, when SOC increases, due to the relation in Eq. (19) the average Fermi wavelength becomes smaller and thus  $\xi_{\min}$  decreases.

*A comparison with other approaches.* So far, several methods have been proposed to solve the Boltzmann equation for isotropic 2DRSs. In the method presented by Xiao *et al.*, by developing the Boltzmann technique they established a set of self-consistent equations for the transport times [11,37]. Their calculations are based on the exact transport time solution (ETTS) of the Boltzmann equation in the Born approximation. In this method, by introducing an isotropic transport time for electrons with energy  $\varepsilon$  in the band  $n$ , via

$$f_n - f_n^0 = \left( \frac{\partial f_n^0}{\partial \varepsilon_n} \right) \mathbf{E} \cdot \mathbf{v}_n(\phi) \tau^n(\varepsilon), \quad (20)$$

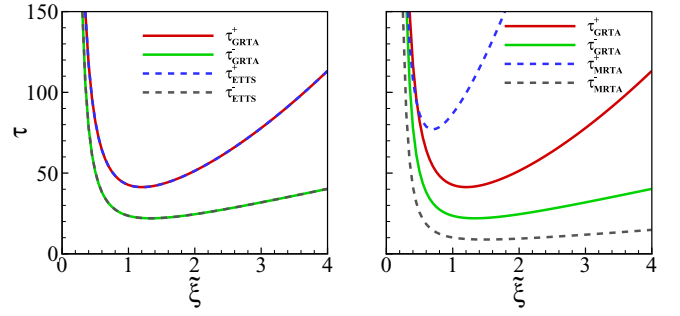


FIG. 5. The relaxation times in the bands + and - vs CMS when  $\tilde{\varepsilon}_R = 0.25$ . Left: The dashed lines are the results of ETTS method, and the solid lines are obtained by GRTA. Right: The dashed lines are the results of MRTA, and the solid lines are obtained by GRTA.

and using the Boltzmann equation, we obtain the following self-consistent equation for the relaxation times:

$$\frac{1}{\tau_{\text{ETTS}}^n(\varepsilon_F)} = \sum_{n'=\pm} \int \frac{d\phi'}{2\pi} w_{n,n'}(\varepsilon_F) \times \left[ 1 - \cos(\Delta\phi) \frac{v_{n'}(\phi')}{v_n(\phi)} \frac{\tau^{n'}(\varepsilon_F)}{\tau^n(\varepsilon_F)} \right]. \quad (21)$$

By solving this integral, we reach two linear equations for the relaxation times  $\tau^+$  and  $\tau^-$  (not shown). In Fig. 5 (left panel), we have plotted the relaxation times obtained by the ETTS method. The results of the GRTA are also plotted for comparison. As is seen, these two methods are completely consistent.

The modified relaxation time approximation (MRTA) is another method for solving the Boltzmann equation for isotropic 2DRSs. In this method, the relaxation time in the band  $n$  is given by [17,36]

$$\frac{1}{\tau_{\text{MRTA}}^n(\varepsilon_F)} = \sum_{n'=\pm} \int \frac{d\phi'}{2\pi} w_{n,n'}(\varepsilon_F) \left[ 1 - \cos(\Delta\phi) \frac{v_{n'}(\phi')}{v_n(\phi)} \right]. \quad (22)$$

In both the ETTS and GRTA methods, we need to solve two coupled equations in order to obtain the relaxation times, while in the MRTA method the band dependence of  $\tau_{\text{MRTA}}$  is neglected. In Fig. 5 (right panel), we have plotted the relaxation times obtained by the MRTA. In the band -, due to the larger Fermi wavelength, we expect the relaxation time to be smaller, but in the GRTA, because of the coupling between the two bands, the relaxation time  $\tau^-$  is larger than the corresponding one in the MRTA. Similarly, in the band +, because of the coupling with the band -, the relaxation time is smaller than the corresponding one in the MRTA. Regardless of the differences in these methods, the behaviors of the relaxation times versus CMS are qualitatively the same. The same discussions are also valid when the Fermi energy is located below the BCP.

### Anisotropic magnetoresistance

When the spins of magnetic clusters are aligned in a direction given by  $\theta$  (see Fig. 2), the system is highly anisotropic and the conductivities in the  $x$  and  $y$  directions behave differently. The conductivity  $\sigma_{xx}$  increases after the minimum and

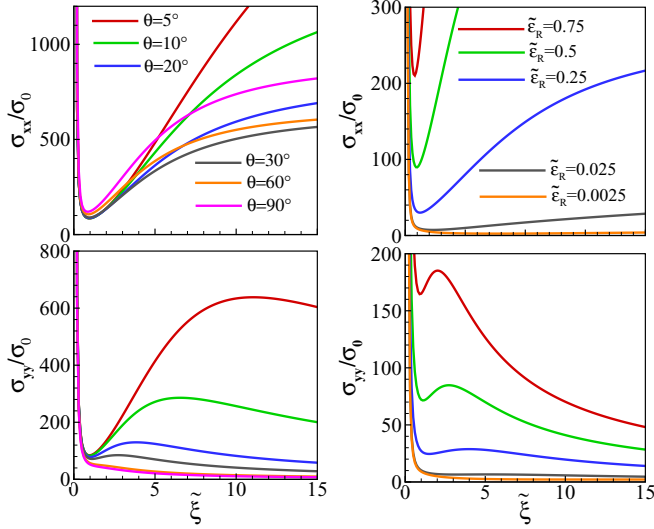


FIG. 6. Left column: The conductivity of the 2DRS along  $x$  and  $y$  directions vs CMS, for different values of the tilt angle  $\theta$ , when  $\tilde{\epsilon}_R = 0.5$ . Right column: The conductivity of the 2DRS along  $x$  and  $y$  directions vs CMS, for different strengths of SOC, when  $\theta = \pi/6$ . Here, Fermi energy is located above the BCP.

saturates at large CMSs; however  $\sigma_{yy}$  decreases by increasing CMS as shown in Fig. 6. Such a different behavior can be explained as follows. When the electric field is applied along the  $x$  axis, most of electrons involved in  $\sigma_{xx}$  move in the  $x$  direction, and due to the spin-orbit locking their spins lie in the  $y$  direction. By increasing the tilt angle  $\theta$ ,  $S_y$  becomes larger and due to the electron-cluster interaction the spin accumulation along the  $y$  axis increases which, in turn, causes the increase of conduction electrons along  $x$  direction. But, for conductivity along  $y$  axis, electrons' spins are perpendicular to  $S_y$ . When  $S_y$  becomes larger, electrons try to align their spin with  $S_y$  to minimize the exchange energy. Again due to the SOC, electrons have to change their direction of motion which leads to a reduction of  $\sigma_{yy}$ .

As an amount of the anisotropy of the system, we investigate the behavior of AMR, defined as

$$\text{AMR} = \frac{\sigma_{xx} - \sigma_{yy}}{\sigma_{xx} + \sigma_{yy}}. \quad (23)$$

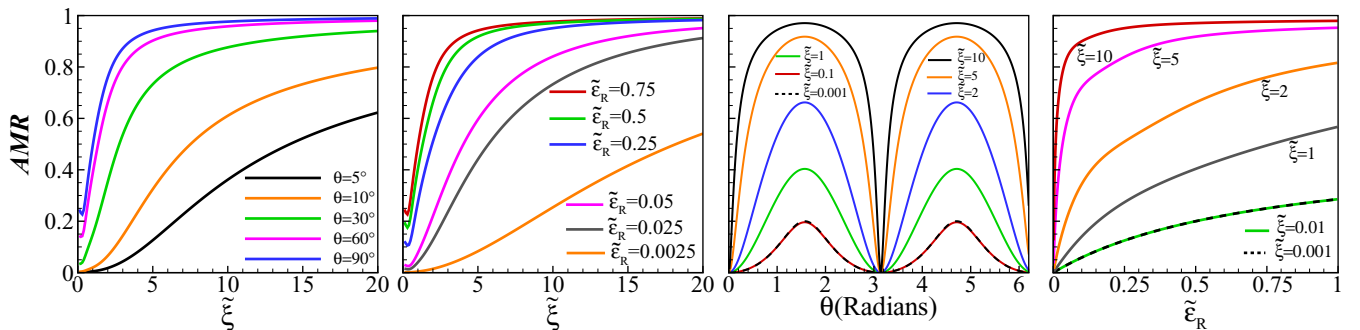


FIG. 7. From left to right: The AMR vs CMS for different values of the tilt angle  $\theta$ , when  $\tilde{\epsilon}_R = 0.75$ . The AMR vs CMS for different strengths of SOC, when  $\theta = \pi/2$ . The AMR vs the tilt angle  $\theta$  for different CMSs, when  $\tilde{\epsilon}_R = 0.5$ . The AMR vs  $\tilde{\epsilon}_R$  for different CMSs, when  $\theta = \pi/2$ .

In Fig. 7, we have plotted the AMR versus CMS, for different values of the tilt angle  $\theta$ , when the strength of SOC is  $\tilde{\epsilon}_R = 0.75$ . By increasing  $\xi$ , the AMR increases monotonically and saturates to unit at large values of  $\xi$ . Also, by increasing the tilt angle  $\theta$  the AMR increases, implying that the system is more anisotropic when clusters' spin lies on the surface of the 2DRS. We have also plotted in Fig. 7 the AMR versus  $\xi$  for different strengths of SOC when  $\theta = \pi/2$ . As is seen, by increasing  $\tilde{\epsilon}_R$  the anisotropy of the system enhances (this behavior, i.e., the increase of AMR by increasing the strength of SOC, occurs only for the regime of  $\epsilon_F > 0$ . In the regime of  $\epsilon_F < 0$  the AMR experiences a minimum at an  $\tilde{\epsilon}_R$ , which will be discussed in next section. In order to see the angular dependence of the AMR, we have also plotted in Fig. 7 the AMR versus  $\theta$ , for different values of CMS, at  $\tilde{\epsilon}_R = 0.5$ . As is seen, the angular dependence of the AMR changes by varying  $\xi$ . The unconventional behavior of the AMR as a function of the tilt angle  $\theta$  is a combined effect of SOC and magnetic clusters. The maximum value of the AMR increases by increasing  $\tilde{\epsilon}_R$ . To show this dependence for very small CMSs, we have also plotted in Fig. 7 the AMR versus  $\tilde{\epsilon}_R$  for different CMSs, at  $\theta = \pi/2$ . As is clearly seen the anisotropy exists even at very small SOC; it grows monotonically by increasing SOC and saturates to 1. This property is not seen in the regime of  $\epsilon_F < 0$ . As we will show in the next section, below the BCP, for small CMSs the AMR is almost constant with respect to  $\tilde{\epsilon}_R$ .

The behavior of the conductivity in 2DRSs is generally similar to the surface conductivity of 3D magnetic topological insulators [21]. However, in contrast to the topological insulators, in 2DRSs  $\xi_{\min}$  strongly depends on the strength of SOC (see Fig. 6). By decreasing the SOC,  $\xi_{\min}$  increases and goes to infinity in the limit of  $\xi \rightarrow 0$ .

#### IV. SINGLE-BAND SCATTERING ( $\epsilon_F < 0$ )

Below the BCP, the conductivity of the 2DRS is obtained as (see Appendix B)

$$\begin{aligned} \sigma_{xx} &= \sigma_0 \sqrt{\tilde{\epsilon}_R - 1} \sum_{\nu=1,2} \tau_x^\nu(|\epsilon_F|) [\sqrt{\tilde{\epsilon}_R} - (-1)^\nu \sqrt{\tilde{\epsilon}_R - 1}], \\ \sigma_{yy} &= \sigma_0 \sqrt{\tilde{\epsilon}_R - 1} \sum_{\nu=1,2} \tau_y^\nu(|\epsilon_F|) [\sqrt{\tilde{\epsilon}_R} - (-1)^\nu \sqrt{\tilde{\epsilon}_R - 1}], \end{aligned} \quad (24)$$

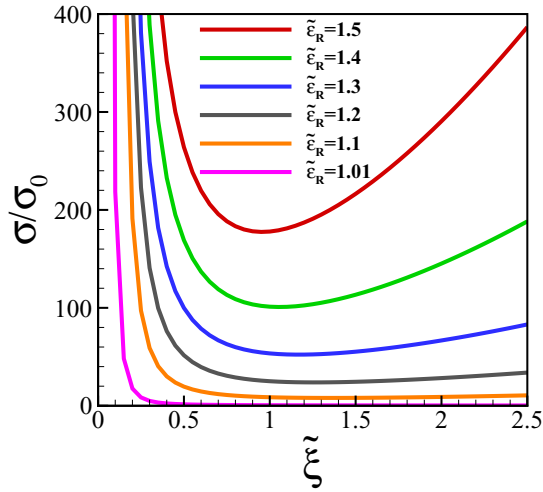


FIG. 8. The conductivity of the isotropic 2DRS for different strengths of SOC, when Fermi energy is located below the BCP ( $-\varepsilon_R/2 < \varepsilon_F < 0$ ).

where  $\tilde{\varepsilon}_R = \varepsilon_R/(2|\varepsilon_F|)$ . In the isotropic case,  $\tau_x^1 = \tau_y^1$  and  $\tau_x^2 = \tau_y^2$ , and the conductivities along the  $x$  and  $y$  directions are identically the same. In Fig. 8, we have plotted the conductivity of the system versus  $\tilde{\xi}$  for different strengths of SOC. Similarly to the two-band case, by increasing  $\tilde{\xi}$  the conductivity decreases rapidly, becomes minimum at  $\tilde{\xi}_{\min} \sim \lambda_F^{av}/2\pi$ , and then increases gradually. Here, the Fermi wavelength of electrons in the branch  $\nu$  is given by  $\lambda_{\nu F} = \lambda_F^0/[\sqrt{\tilde{\varepsilon}_R} - (-1)^\nu\sqrt{\tilde{\varepsilon}_R - 1}]$  and the average Fermi wavelength is given by  $\lambda_F^{av} = \lambda_F^0/\sqrt{\tilde{\varepsilon}_R}$ . In contrast to the two-band case, below the BCP the conductivity decreases by decreasing the SOC and goes toward zero in the limit of  $\tilde{\varepsilon}_R \rightarrow 1$ . Actually, by decreasing SOC the numbers of electrons with the same  $k$  ( $k_{1F} \approx k_{2F}$ ) but opposite velocities are almost equal and consequently conductivity is zero. In contrast, above the BCP the velocities in the bands  $+$  and  $-$  are always in the same directions and the system possesses a nonzero conductivity.

#### Anisotropic case ( $\theta \neq 0$ )

Below the BCP the behavior of the conductivities  $\sigma_{xx}$  and  $\sigma_{yy}$ , is generally the same as the corresponding ones above the BCP. However, there are some obvious contrasts between these two regimes, which are seen in the behavior of the AMR. In Fig. 9, we have plotted the AMR of the system versus  $\tilde{\xi}$ , for different strengths of SOC and various tilt angles  $\theta$ . Unlike the two-band case, for a given  $\theta$  the starting point of the AMR at  $\tilde{\xi} = 0$  is independent of SOC. The behavior of the AMR with respect to CMS is not monotonic for different strengths of SOC. In order to demonstrate such a nonmonotonic behavior, we have also plotted in Fig. 10 the AMR versus  $\tilde{\varepsilon}_R$  for different values of  $\tilde{\xi}$  and various tilt angles  $\theta$ . For small CMSs, unlike the two-band case, the AMR is almost independent of  $\tilde{\varepsilon}_R$  and the SOC does not have significant effects on the anisotropy of the system. By increasing CMS the AMR becomes more sensitive to  $\tilde{\varepsilon}_R$ : it decreases by increasing  $\tilde{\varepsilon}_R$ , becomes minimum, and then increases to a value less than 1 (this value depends on the CMS). When CMS increases

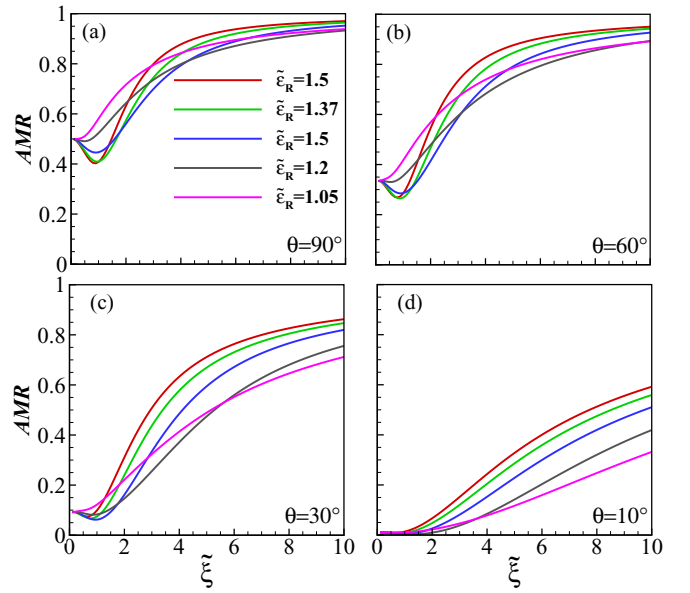


FIG. 9. The AMR vs CMS for different strengths of SOC.

the minimum approaches the point  $\tilde{\varepsilon}_R = 1$ . For larger CMSs this minimum disappears and independently of the strength of SOC the AMR becomes almost 1. The reason behind such kind of behavior can be understood by looking at the direction of electric current in the presence of an electric field. When a field is applied along the  $x$  axis, two types of currents are generated in the system: one is by electrons with wave vector  $\mathbf{k}_{1F}$  along the  $x$  axis, and the other is by electrons with wave vector  $\mathbf{k}_{2F}$  in the  $-x$  direction. Since the current in branch 1 is larger than 2, a net current flows along the  $x$  direction. Moreover, the Fermi wavelength  $\lambda_{1F}$  is smaller than  $\lambda_{2F}$  for all values of  $\tilde{\varepsilon}_R > 1$ ; therefore for a given  $\tilde{\xi}$ , by varying  $\tilde{\varepsilon}_R$  electrons with  $k_{1F}$  reaches the efficient scattering

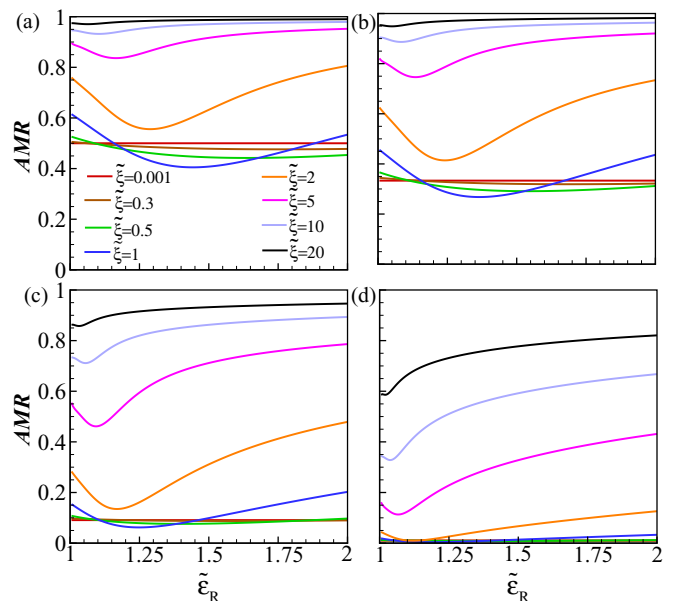


FIG. 10. The AMR versus the strength of SOC, for different CMSs, when (a)  $\theta = 90^\circ$ , (b)  $\theta = 60^\circ$ , (c)  $\theta = 30^\circ$ , and (d)  $\theta = 10^\circ$ .

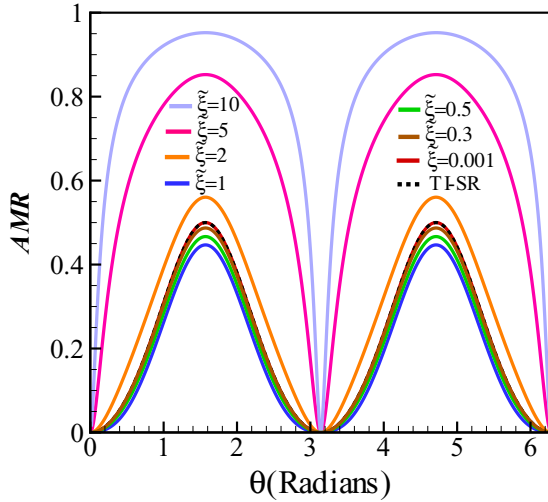


FIG. 11. The AMR as a function of the tilt angle  $\theta$ , for different CMSs, when  $\tilde{\epsilon}_R = 1.25$ . The black dashed line is for TIs doped with magnetic impurities, where the scattering potential is the Dirac  $\delta$  function.

point where  $\lambda_{1F} \sim 2\pi\xi$ , and due to the maximum scattering of electrons in branch 1 and also the negative conductivity of electrons in branch 2,  $\sigma_{xx}$  is minimum. By increasing  $\tilde{\epsilon}_R$ , Fermi wavelength of electrons in branch 1 decreases, and positive conductivity along  $x$  axis begins to be enhance. These variations in  $\sigma_{xx}$  cause a minimum to emerge in the AMR versus  $\tilde{\epsilon}_R$ . By applying the electric field along the  $y$  axis, the variations of  $\sigma_{yy}$  are exactly the same as  $\sigma_{xx}$ , but since  $\sigma_{xx}$  is larger than  $\sigma_{yy}$ , it has a dominant contribution on the AMR. By decreasing  $\tilde{\epsilon}_R$  the Fermi wavelength of electrons in branch 1 increases and hence the minimum approaches the point  $\tilde{\xi} = 0$ . Also, for large enough CMSs, the Fermi wavelength of electrons in branch 1 remains always smaller than  $\tilde{\xi}$  and no efficient scattering occurs for electrons in this branch, so by increasing  $\tilde{\xi}$  this minimum disappears and for very large values of  $\tilde{\xi}$  the AMR saturates to 1. For large values of  $\tilde{\epsilon}_R$ , the Fermi wavelength of electrons in branch 1 becomes smaller, and by a decrease of the CMS the minimum location approaches infinity and the AMR becomes a constant (this constant is determined by the clusters' tilt angle). The main reason for this behavior is the anisotropic band structure below the BCP.

Figure 11 shows the angular dependence of the AMR. Like the two-band case, the AMR behaves unconventionally for large CMSs (for  $\tilde{\xi}$  almost larger than 1). For small CMSs the AMR is given by

$$\text{AMR} = \sin^2 \theta / (2 + \cos^2 \theta), \quad (25)$$

which is nothing but the AMR of 3D magnetic topological insulators with short-range Dirac  $\delta$  scattering potential [21,40].

## V. SUMMARY AND CONCLUSION

We presented a comprehensive study of the transport properties of 2DRSs with strong SOC doped with interacting magnetic impurities. Exchange interactions between magnetic impurities cause the formation of magnetic clusters whose

mean sizes (CMSs) and number (CN) depend on temperature. Treating magnetic clusters as scattering centers and modeling the interaction of itinerant electrons with magnetic clusters by a long-range scattering potential, we demonstrated that the combined effects of Rashba SOC and magnetic clusters cause the system to be anisotropic. Using a semiclassical Boltzmann approach we computed the relaxation times, the conductivities, and the AMRs of the system in both regimes of above and below the BCP. We demonstrated the following: (i) In the isotropic case the conductivity is a nonmonotonic function of CMS: it decreases by increasing CMS, becomes minimum at  $\tilde{\xi}_{min}$ , and then increases by CMS. By increasing the strength of SOC the conductivity increases for all CMSs. (ii) In the anisotropic case, the AMR strongly depends on the CMS: it increases by increasing CMS and saturates to unit at large CMSs. Moreover, the angular dependence of the AMR is unconventional in comparison with the well-known  $\cos^2 \theta$  angular dependence seen in ferromagnets. For small CMSs, below the BCP the angular dependence of the AMR is consistent with 3D magnetic topological insulators. (iii) In contrast to the two-band regime in which the AMR always increases by increasing the strengths of SOC, in the single-band regime it experiences a minimum at an  $\tilde{\epsilon}_R$  which strongly depends on the CMS. For small CMSs, in the single-band regime the AMR is almost constant and does not change by varying  $\tilde{\epsilon}_R$ ; however in the two-band regime the AMR strongly depends on the strength of SOC even at small CMSs.

Both the CMS and CN depend on temperature. By knowing their temperature dependence, the temperature dependence of conductivities can be obtained, which is crucial in investigation of the thermoelectric properties of the 2DRSs. The temperature dependencies of the CMS and CN can be obtained using Monte Carlo simulations, which are left for future study.

## APPENDIX A: THE CONDUCTIVITY OF 2DRS ABOVE THE BCP

When the Fermi energy is located above the BCP, both bands are involved in the transport properties of the 2DRS, and we should take the contributions of backscatterings and intra-band scatterings into account in computing the nonequilibrium distribution functions ( $f_+$  and  $f_-$ ). Substituting Eq. (11) into (10), and writing  $\mathbf{E} \cdot \mathbf{v}_n$  as  $E v_n \cos(\phi - \chi)$ , we achieve the following integral equations:

$$\begin{aligned} \cos \phi &= \bar{w}_+(\phi) a_+(\phi) - \int d\phi' [w_{++}(\phi, \phi') a_+(\phi') \\ &\quad + w_{+-}(\phi, \phi') a_-(\phi')], \\ \cos \phi &= \bar{w}_-(\phi) a_-(\phi) - \int d\phi' [w_{--}(\phi, \phi') a_-(\phi') \\ &\quad + w_{-+}(\phi, \phi') a_+(\phi')], \end{aligned} \quad (A1)$$

$$\begin{aligned} \sin \phi &= \bar{w}_+(\phi) b_+(\phi) - \int d\phi' [w_{++}(\phi, \phi') b_+(\phi') \\ &\quad + w_{+-}(\phi, \phi') b_-(\phi')], \\ \sin \phi &= \bar{w}_-(\phi) b_-(\phi) - \int d\phi' [w_{--}(\phi, \phi') b_-(\phi') \\ &\quad + w_{-+}(\phi, \phi') b_+(\phi')], \end{aligned} \quad (A2)$$



where  $w_{n,n'}(\phi, \phi') = A(2\pi)^{-2} \int k' dk' w_{n,n'}(\mathbf{k}, \mathbf{k}')$ , and  $\bar{w}_n(\phi) = \int d\phi' [w_{+n}(\phi, \phi') + w_{-n}(\phi, \phi')]$ . Using Fermi's golden rule, the transition rate is written in terms of the scattering amplitude  $|T_{n,n'}(\mathbf{k}, \mathbf{k}')|^2$  as

$$w_{n,n'}(\mathbf{k}, \mathbf{k}') = \frac{2\pi}{\hbar} |T_{n,n'}(\mathbf{k}, \mathbf{k}')|^2 \delta(\varepsilon_{nk} - \varepsilon_{n'k'}). \quad (\text{A3})$$

Within the first Born approximation, the  $T$  matrix is given by  $T_{n,n'}(\mathbf{k}, \mathbf{k}') \approx \langle n\mathbf{k} | \mathcal{H}_{\sigma S} | n'\mathbf{k}' \rangle$ , where  $\mathcal{H}_{\sigma S}$  is the scattering Hamiltonian, given by  $\mathcal{H}_{\sigma S} = \sum_{\mathbf{r}, \mathbf{R}} H_{\sigma S}$ . Since magnetic

clusters are uncorrelated and distributed randomly on the 2DRS, one can show that  $\langle |T_{n,n'}(\mathbf{k}, \mathbf{k}')|^2 \rangle_{ens} = \eta_c |H_{\sigma S}(\mathbf{k} - \mathbf{k}')|^2$ , where  $\langle \dots \rangle_{ens}$  denotes ensemble average, and  $H_{\sigma S}(\mathbf{k} - \mathbf{k}')$  is the Fourier transformation of Eq. (7) at  $\mathbf{R} = 0$ . As the unperturbed Hamiltonian in Eq. (1) is gapless and the time-reversal symmetry is preserved in the system, other mechanisms such as skew scattering, anomalous velocity, and side jump have vanishing contributions to the transport properties of the system (anomalous Hall conductivity is zero) and the lowest-order Born approximation gives reliable results for the transport of the system [41].

By considering elasticity of the scattering we obtain

$$w_{n,n'} = \omega_0 \frac{N_n}{N_0} \xi^4 \frac{1 - nn'(\cos 2\theta \cos \phi \cos \phi' + \sin \phi \sin \phi')}{(1 + \xi^2[k_n^2 + k_{n'}^2])^3 (1 - \Omega_{n,n'} \cos \Delta\phi)^3},$$

$$\bar{w}_n(\phi) = \omega_0 \sum_{n'=\pm} \frac{\tilde{\xi}^4 (1 + n' \sqrt{\frac{\varepsilon_R/2\varepsilon}{\varepsilon_R/2\varepsilon+1}})}{(1 + \xi^2[k_n^2 + k_{n'}^2])^3 (1 - \Omega_{n,n'}^2)^{\frac{5}{2}}} \left[ \frac{3}{2} \pi nn' \Omega_{n,n'} \sin^2 \theta \cos 2\phi + \pi (2 + \Omega_{n,n'}^2 - 3nn' \cos^2 \theta) \right], \quad (\text{A4})$$

where  $\Omega_{n,n'} = \frac{2\xi^2 k_n k_{n'}}{1 + \xi^2[k_n^2 + k_{n'}^2]}$ ,  $\omega_0 = \frac{\pi \hbar n_c J_0^2 S^2}{4Am\varepsilon_F}$ , and  $\tilde{\xi} = \xi \sqrt{2m\varepsilon_F/\hbar^2}$ .

In order to solve Eqs. (A1) and (A2), we employ the Fourier expansions of  $a_{\pm}(\phi)$  and  $b_{\pm}(\phi)$  as

$$a_{\pm}(\phi) = \sum_{m=0}^{\infty} c_{2m+1}^{\pm} \cos[(2m+1)\phi], \quad (\text{A5})$$

$$b_{\pm}(\phi) = \sum_{m=0}^{\infty} s_{2m+1}^{\pm} \sin[(2m+1)\phi], \quad (\text{A6})$$

which satisfy the particle number conservation. Since the functions  $w_{n,n'}(\phi, \phi')$  and  $\bar{w}_n(\phi)$  are invariant under the transformations  $(\phi, \phi') \rightarrow (-\phi, -\phi')$  and  $(\phi, \phi') \rightarrow (\pi - \phi, \pi - \phi')$ , the functions  $a_{\pm}(\phi)$  and  $b_{\pm}(\phi)$  should satisfy the relations  $a_{\pm}(-\phi) = a_{\pm}(\phi)$ ,  $a_{\pm}(\pi - \phi) = -a_{\pm}(\phi)$ ,  $b_{\pm}(-\phi) = -b_{\pm}(\phi)$ , and  $b_{\pm}(\pi - \phi) = b_{\pm}(\phi)$ ; hence only the Fourier coefficients  $c_i^{\pm}$  and  $s_i^{\pm}$  with odd  $i$  have appeared in the above expansions.  $c_{2m+1}^{\pm}$  and  $s_{2m+1}^{\pm}$  have a dimension of time and depend on the CMS, the CN, the tilt angle  $\theta$ , and the Rashba energy  $\varepsilon_R$ . By substituting Eq. (A5) into both relations in Eq. (A1), we obtain the following set of linear equations for the coefficients  $c_i^{\pm}$ :

$$\begin{bmatrix} \mathbf{A}_0 & \mathbf{C}_1 & \mathbf{0} & \dots & \dots & \dots & \dots \\ \mathbf{C}_1 & \mathbf{A}_1 & \mathbf{C}_2 & \mathbf{0} & \dots & \dots & \dots \\ \mathbf{0} & \mathbf{C}_2 & \mathbf{A}_2 & \mathbf{C}_3 & \mathbf{0} & \dots & \dots \\ \mathbf{0} & \mathbf{0} & \mathbf{C}_3 & \mathbf{A}_3 & \mathbf{C}_4 & \mathbf{0} & \dots \\ \mathbf{0} & \mathbf{0} & \mathbf{0} & \mathbf{C}_4 & \mathbf{A}_4 & \mathbf{C}_5 & \dots \\ \vdots & \vdots & \vdots & \vdots & \vdots & \ddots & \ddots \end{bmatrix} \begin{bmatrix} \mathbf{c}_1 \\ \mathbf{c}_3 \\ \mathbf{c}_5 \\ \mathbf{c}_7 \\ \mathbf{c}_9 \\ \vdots \end{bmatrix} = 1/\omega_0 \begin{bmatrix} \mathbf{d}_1 \\ \mathbf{d}_3 \\ \mathbf{d}_5 \\ \mathbf{d}_7 \\ \mathbf{d}_9 \\ \vdots \end{bmatrix}, \quad (\text{A7})$$

where the matrix elements are the following  $2 \times 2$  matrices:

$$\mathbf{A}_0 = \begin{bmatrix} L_0^+ + K_0^+ & G_0^- + D_0^- \\ G_0^+ + D_0^+ & L_0^- + K_0^- \end{bmatrix}, \quad (\text{A8})$$

and

$$\mathbf{A}_m = \begin{bmatrix} K_m^+ & D_m^- \\ D_m^+ & K_m^- \end{bmatrix}, \quad \mathbf{C}_m = \begin{bmatrix} L_m^+ & G_m^- \\ G_m^+ & L_m^- \end{bmatrix}, \quad (\text{A9})$$

where  $L_m^\pm$ ,  $K_m^\pm$ ,  $G_m^\pm$ , and  $D_m^\pm$  are the following dimensionless functions:

$$\begin{aligned}
 L_m^\pm(\varepsilon, \xi, \theta)/\tilde{\xi}^4 &= \kappa_{\pm\pm} + \kappa_{\pm\mp} - \frac{F(m, \Omega_{\pm\pm})(1 - \cos 2\theta)(1 \pm \sqrt{\frac{\varepsilon_R/2\varepsilon}{\varepsilon_R/2\varepsilon+1}})}{(1 + 2\xi^2 k_\pm^2)^3}, \\
 K_m^\pm(\varepsilon, \xi, \theta)/\tilde{\xi}^4 &= \mu_{\pm\pm} + \mu_{\pm\mp} - \frac{[Q(m, \Omega_{\pm\pm}) - \{F(m, \Omega_{\pm\pm}) + F(m + 1, \Omega_{\pm\pm})\}](1 + \cos 2\theta)(1 \pm \sqrt{\frac{\varepsilon_R/2\varepsilon}{\varepsilon_R/2\varepsilon+1}})}{(1 + 2\xi^2 k_\pm^2)^3}, \\
 G_m^\pm(\varepsilon, \xi, \theta)/\tilde{\xi}^4 &= \frac{F(m, \Omega_{\pm\mp})(1 - \cos 2\theta)(1 \pm \sqrt{\frac{\varepsilon_R/2\varepsilon}{\varepsilon_R/2\varepsilon+1}})}{(1 + \xi^2[k_\pm^2 + k_\mp^2])^3}, \\
 D_m^\pm(\varepsilon, \xi, \theta)/\tilde{\xi}^4 &= -\frac{[Q(m, \Omega_{\pm\mp}) + \{F(m, \Omega_{\pm\mp}) + F(m + 1, \Omega_{\pm\mp})\}](1 + \cos 2\theta)(1 \pm \sqrt{\frac{\varepsilon_R/2\varepsilon}{\varepsilon_R/2\varepsilon+1}})}{(1 + \xi^2[k_\pm^2 + k_\mp^2])^3},
 \end{aligned}
 \tag{A10}$$

where

$$\kappa_{nn'} = \frac{\frac{3}{2}\pi nn' \Omega_{n,n'} \sin^2 \theta (1 + n' \sqrt{\frac{\varepsilon_R/2\varepsilon}{\varepsilon_R/2\varepsilon+1}})}{(1 + \xi^2[k_n^2 + k_{n'}^2])^3 (1 - \Omega_{n,n'}^2)^{\frac{5}{2}}},
 \tag{A11}$$

$$\mu_{mm'} = \frac{\pi(2 + \Omega_{n,n'}^2 - 3nn' \cos^2 \theta)(1 + n' \sqrt{\frac{\varepsilon_R/2\varepsilon}{\varepsilon_R/2\varepsilon+1}})}{(1 + \xi^2[k_n^2 + k_{n'}^2])^3 (1 - \Omega_{n,n'}^2)^{\frac{5}{2}}},
 \tag{A12}$$

and

$$\begin{aligned}
 F(m, y) &= \sum_{l=0}^{\infty} \frac{\pi(2l + 2)!}{4(l - m)!(l + m)!} \left(\frac{y}{2}\right)^{2l} = \sum_{k=0}^{\infty} \frac{\pi(2m + 2k + 2)!}{4k!(2m + k)!} \left(\frac{y}{2}\right)^{2m+2k} \\
 &= \frac{\pi(1 + m)(1 + 2m)}{2} \left(\frac{y}{2}\right)^{2m} {}_2F_1\left[\frac{3}{2} + m, 2 + m, 1 + 2m, y^2\right], \\
 Q(m, y) &= \sum_{l=0}^{\infty} \frac{\pi(2l + 3)!}{(l - m)!(l + m + 1)!} \left(\frac{y}{2}\right)^{2l+1} = \sum_{k=0}^{\infty} \frac{\pi(2m + 2k + 3)!}{k!(2m + k + 1)!} \left(\frac{y}{2}\right)^{2m+2k+1} \\
 &= 2\pi(m + 1)(3 + 2m) \left(\frac{y}{2}\right)^{2m+1} {}_2F_1\left[2 + m, \frac{5}{2} + m, 2 + 2m, y^2\right].
 \end{aligned}
 \tag{A13}$$

Here,  ${}_2F_1[\frac{3}{2} + m, 2 + m, 1 + 2m, y^2]$  and  ${}_2F_1[2 + m, \frac{5}{2} + m, 2 + 2m, y^2]$  are hypergeometric functions. Since for  $\varepsilon_R/\varepsilon_F \geq 0$ , we have  $0 \leq \Omega_{n,n'} < 1$ , the functions  $F(m, \Omega_{n,n'})$  and  $Q(m, \Omega_{n,n'})$  are simplified as

$$\begin{aligned}
 F(m, \Omega_{n,n'}) &= \frac{\pi[2 + \Omega_{n,n'}^2 + 6m\sqrt{1 - \Omega_{n,n'}^2} - 4m^2(1 - \Omega_{n,n'}^2)]}{4\Omega_{n,n'}^{-2m}(1 + \sqrt{1 - \Omega_{n,n'}^2})^{2m}(1 - \Omega_{n,n'}^2)^{\frac{5}{2}}}, \\
 Q(m - 1, \Omega_{n,n'}) &= \frac{3\pi - 3\pi\sqrt{1 - \Omega_{n,n'}^2}(1 - 2m) + 4\pi m(m - 1)(1 - \Omega_{n,n'}^2)}{\Omega_{n,n'}^{1-2m}(1 + \sqrt{1 - \Omega_{n,n'}^2})^{2m-1}(1 - \Omega_{n,n'}^2)^{\frac{5}{2}}}.
 \end{aligned}
 \tag{A14}$$

The vectors  $\mathbf{c}_m$  and  $\mathbf{d}_m$  in Eq. (A7) are the following two-component vectors:

$$\mathbf{c}_m = \begin{bmatrix} c_m^+ \\ c_m^- \end{bmatrix}, \mathbf{d}_m = \begin{cases} \begin{bmatrix} 1 \\ 1 \end{bmatrix}, & m > 1, \\ \mathbf{0}, & m = 1. \end{cases}
 \tag{A15}$$

For solving the linear equations in (A7), we have to truncate the series (A5) at some point. For an specified  $\xi$ ,  $\theta$ , and  $\varepsilon_R$ , by selecting a proper number of trigonometric functions in the series (A5), we obtain the  $a_+(\phi)$  and  $a_-(\phi)$  functions, precisely [21].

By selecting the first  $j$ -independent trigonometric functions, the matrix equation (A7) reduces to

$$\begin{bmatrix} \mathbf{A}_0 & \mathbf{C}_1 & \mathbf{0} & \mathbf{0} & \cdots & \mathbf{0} \\ \mathbf{C}_1 & \mathbf{A}_1 & \mathbf{C}_2 & \mathbf{0} & \cdots & \mathbf{0} \\ \mathbf{0} & \mathbf{C}_2 & \mathbf{A}_2 & \mathbf{C}_3 & \cdots & \vdots \\ \vdots & \vdots & \vdots & \vdots & \vdots & \mathbf{0} \\ \mathbf{0} & \cdots & \mathbf{0} & \mathbf{C}_{j-1} & \mathbf{A}_{j-1} & \mathbf{C}_j \\ \mathbf{0} & \cdots & \mathbf{0} & \mathbf{0} & \mathbf{C}_j & \mathbf{A}_j \end{bmatrix} \begin{bmatrix} \mathbf{c}_1 \\ \mathbf{c}_3 \\ \mathbf{c}_5 \\ \vdots \\ \mathbf{c}_{2j-1} \\ \mathbf{c}_{2j+1} \end{bmatrix} = 1/\omega_0 \begin{bmatrix} \mathbf{d}_1 \\ \mathbf{d}_3 \\ \mathbf{d}_5 \\ \vdots \\ \mathbf{d}_{2j-1} \\ \mathbf{d}_{2j+1} \end{bmatrix}. \quad (\text{A16})$$

Now we have a set of  $j + 1$  equations with  $j + 1$  variables. Since  $\mathbf{d}_{2j+1} = \mathbf{0}$  for  $j \geq 1$ , we begin with the two last equations  $j + 1$  and  $j$ ; then by eliminating the coefficient  $\mathbf{c}_{2j+1}$  we reach the following equation:

$$\mathbf{C}_j^{-1} \cdot \mathbf{C}_{j-1} \cdot \mathbf{c}_{[2(j-2)+1]} + \Delta_j \cdot \mathbf{c}_{[2(j-1)+1]} = 0, \quad (\text{A17})$$

where

$$\Delta_j = \mathbf{C}_j^{-1} \cdot \mathbf{A}_{j-1} - \mathbf{A}_j^{-1} \cdot \mathbf{C}_j. \quad (\text{A18})$$

By using the  $(j - 1)$ th equation of (A16) and Eq. (A17) we can eliminate the coefficient  $\mathbf{c}_{2j-1}$ . Repeating this method to the first equation of (A16) we reach

$$\omega_0 \mathbf{c}_1 = (\Delta_1^+)^{-1} \cdot \mathbf{C}_1^{-1} \cdot \mathbf{d}_1, \quad (\text{A19})$$

where

$$\Delta_i^+ = \mathbf{C}_i^{-1} \cdot \mathbf{A}_{i-1} - (\Delta_{i+1}^+)^{-1} \cdot \mathbf{C}_{i+1}^{-1} \cdot \mathbf{C}_i. \quad (\text{A20})$$

By obtaining  $\mathbf{c}_1$  from Eq. (A19) and substituting it into Eq. (A7), the other  $\mathbf{c}_i$  vectors, and finally the functions  $a_{\pm}(\phi)$ , are obtained in terms of  $k$ ,  $\alpha$ ,  $\xi$ ,  $\theta$ , and  $\eta_c$ .

By the same procedure, we have also obtained the functions  $b_{\pm}(\phi)$  in terms of the nonzero coefficients  $s_i^{\pm} = s_i^{\pm}(k, \alpha, \xi, \theta, \eta_c)$ , with odd  $i$ . All these nonzero coefficients are given in terms of  $\mathbf{s}_1$  by the relation

$$\omega_0 \mathbf{s}_1 = (\Delta_1^-)^{-1} \cdot \mathbf{C}_1^{-1} \cdot \mathbf{d}_1, \quad (\text{A21})$$

where  $\mathbf{s}_m = \begin{bmatrix} s_m^+ \\ s_m^- \end{bmatrix}$ , and

$$\Delta_1^- = \mathbf{C}_1^{-1} \cdot \mathbf{B}_0 - (\Delta_2^+)^{-1} \cdot \mathbf{C}_2^{-1} \cdot \mathbf{C}_1, \quad (\text{A22})$$

with

$$\mathbf{B}_0 = \begin{bmatrix} K_0^+ - L_0^+ & D_0^- - G_0^- \\ D_0^+ - G_0^+ & K_0^- - L_0^- \end{bmatrix}. \quad (\text{A23})$$

## APPENDIX B: THE CONDUCTIVITY OF THE 2DRS BELOW THE BCP

When the Fermi energy is located in the interval  $-\varepsilon_R/2 < \varepsilon_F < 0$ , we have unconventional intraband and interband

scatterings in the band  $+$ , with the scattering rate

$$w_{\nu, \nu'} = \omega_0 \frac{N_{\nu}}{N_0} \xi^4 \frac{1 - \cos 2\theta \cos \phi \cos \phi' - \sin \phi \sin \phi'}{(1 + \xi^2 [k_{\nu}^2 + k_{\nu'}^2])^3 (1 - \Gamma_{\nu, \nu'} \cos \Delta \phi)^3},$$

$$\bar{w}_{\nu}(\phi) = \omega_0 \sum_{\nu'} \frac{\xi^4 [(-1)^{1+\nu-\nu'} + \sqrt{\frac{\varepsilon_R/2|\varepsilon|}{\varepsilon_R/2|\varepsilon|-1}}]}{(1 + \xi^2 [k_{\nu}^2 + k_{\nu'}^2])^3 (1 - \Gamma_{\nu, \nu'}^2)^{\frac{5}{2}}}$$

$$\times \left[ \frac{3}{2} \pi \Gamma_{\nu, \nu'} \sin^2 \theta \cos 2\phi + \pi (2 + \Gamma_{\nu, \nu'}^2 - 3 \cos^2 \theta) \right], \quad (\text{B1})$$

with  $\Gamma_{\nu, \nu'} = \frac{2\xi^2 k_{\nu} k_{\nu'}}{1 + \xi^2 [k_{\nu}^2 + k_{\nu'}^2]}$ . In order to obtain the nonequilibrium distribution functions of electrons in branches 1 and 2, we should solve two equations like (A1) and (A2). Because of the nonmonotonic dispersion of the band  $+$ , below the BCP the band velocity of electrons is not always parallel to their  $\mathbf{k}$  vector. In order to include this issue in our calculations, we replace  $\phi$  by  $\Phi_{\nu}(\phi)$ , defined by  $\mathbf{v}_{\nu}(\varepsilon, \phi) = v_{\nu}(\varepsilon, \phi)(\cos \Phi_{\nu}, \sin \Phi_{\nu})$ , where  $\Phi_1 = \phi$  and  $\Phi_2 = \phi + \pi$ . Therefore, according to the relation  $\mathbf{v}_{\nu} = (-1)^{\nu} \frac{\hbar}{m} (N_0/N_{\nu}) \mathbf{k}_{\nu}$ , and the method used to obtain the nonequilibrium distribution functions, we define the nonequilibrium distribution functions of electrons in the branch  $\nu$  as (see Appendix C)

$$f_{\nu} - f_{\nu}^0 = eE v_{\nu} \left( \frac{\partial f_{\nu}^0}{\partial \varepsilon_{\nu}} \right) [a_{\nu}(\Phi_{\nu}) \cos \chi + b_{\nu}(\Phi_{\nu}) \sin \chi], \quad (\text{B2})$$

where  $a_{\nu}(\Phi_{\nu})$  and  $b_{\nu}(\Phi_{\nu})$  satisfy the following relations:

$$\cos \Phi_2 = \bar{w}_2(\phi) a_2(\Phi_2) - \int d\phi' [w_{2,2}(\phi, \phi') a_2(\Phi_2') + w_{2,1}(\phi, \phi') a_1(\Phi_1')],$$

$$\cos \Phi_1 = \bar{w}_1(\phi) a_1(\Phi_1) - \int d\phi' [w_{1,1}(\phi, \phi') a_1(\Phi_1') + w_{1,2}(\phi, \phi') a_2(\Phi_2')], \quad (\text{B3})$$

$$\sin \Phi_2 = \bar{w}_2(\phi) b_2(\Phi_2) - \int d\phi' [w_{2,2}(\phi, \phi') b_2(\Phi_2') + w_{2,1}(\phi, \phi') b_1(\Phi_1')],$$

$$\sin \Phi_1 = \bar{w}_1(\phi) b_1(\Phi_1) - \int d\phi' [w_{1,1}(\phi, \phi') b_1(\Phi_1') + w_{1,2}(\phi, \phi') b_2(\Phi_2')]. \quad (\text{B4})$$

For solving the coupled Eqs. (B3) and (B4), the same as the two-band case, we use the Fourier expansions of  $a_{\nu}(\Phi_{\nu})$  and

$b_\nu(\Phi_\nu)$ , and achieve

$$\begin{aligned} a_\nu(\Phi_\nu) &= \sum_{m=0}^{\infty} c_{2m+1}^\nu \cos[(2m+1)\Phi_\nu], \\ b_\nu(\Phi_\nu) &= \sum_{m=0}^{\infty} s_{2m+1}^\nu \sin[(2m+1)\Phi_\nu], \end{aligned} \quad (\text{B5})$$

where  $c_{2m+1}^\nu$  and  $s_{2m+1}^\nu$  are coefficients with a dimension of time. By using the relation (12), and considering the orthogonality of trigonometric functions, the conductivity for  $-\frac{\varepsilon_R}{2} < \varepsilon_F < 0$  is obtained in terms of only the first coefficients of the expansions,  $c_1^\nu$  and  $s_1^\nu$ . As mentioned in the two-band case, these coefficients act as momentum relaxation times of free electrons and can be regarded as effective relaxation times along the  $x$  and  $y$  directions. By defining  $\tau_x^\nu = \omega_0 c_1^\nu$  and  $\tau_y^\nu = \omega_0 s_1^\nu$  we obtain the conductivities of the 2DRS, as in Eq. (24).

### APPENDIX C: BOLTZMANN EQUATION BELOW THE BCP

In elastic scatterings, the magnitude of electron velocity  $v$  does not change, and the nonequilibrium distribution function of electrons in anisotropic systems depends on the angle of velocity with  $x$  axis ( $\Phi$ ). The nonequilibrium distribution function can be written up to the linear order of the electric field as follows [42]:

$$f - f^0 = e \left( \frac{\partial f^0}{\partial \varepsilon} \right) v_{\mathbf{k}} \mathbf{E} \cdot \boldsymbol{\tau}(\Phi), \quad (\text{C1})$$

where  $\boldsymbol{\tau}(\Phi)$  is the relaxation time vector. In order to obtain the relaxation time vector we define the coefficients  $a(\phi)$  and  $b(\phi)$

as relaxation times along the  $x$  and  $y$  axes, and write Eq. (C1) in the form of Eq. (B2) for each branch. In order to use the relation (B2) in the Boltzmann equation, we need to write  $\Phi_\nu$  (the angle of the velocity of electrons in the branch  $\nu$  with  $x$  axis) in terms of  $\phi$ , the polar angle of the  $\mathbf{k}$  vector. In the systems with monotonic band structure, the electron velocity  $\mathbf{v}$  is always parallel to the  $\mathbf{k}$  vector and  $\Phi_\nu = \phi$ . But in 2DRSs with strong Rashba SOC, below the BCP, the electron velocity and wave vector are not always in the same direction and depending on the branch band,  $\mathbf{v}$  is parallel or antiparallel to the  $\mathbf{k}$ . By considering the relation  $\Phi_\nu = \phi + [1 + (-1)^\nu]\pi/2$ , according to the angular dependence of the functions  $a_\nu(\Phi_\nu)$  and  $b_\nu(\Phi_\nu)$  on  $\Phi_\nu$  [ $a_\nu(\Phi)$  and  $b_\nu(\Phi)$  respectively depend on cosine and sine functions], the relations in Eqs. (B3) and (B4) reduce to the following equations:

$$\begin{aligned} \cos \phi &= \bar{w}_\nu(\phi) a_\nu(\phi) \\ &- \sum_{\nu'} \int d\phi' w_{\nu,\nu'}(\phi, \phi') (-1)^{\nu-\nu'} a_{\nu'}(\phi'), \end{aligned} \quad (\text{C2})$$

$$\begin{aligned} \sin \phi &= \bar{w}_\nu(\phi) b_\nu(\phi) \\ &- \sum_{\nu'} \int d\phi' w_{\nu,\nu'}(\phi, \phi') (-1)^{\nu-\nu'} b_{\nu'}(\phi'). \end{aligned} \quad (\text{C3})$$

As in the two-band scattering case, by employing the Fourier series of  $a_\nu(\phi)$  and  $b_\nu(\phi)$  and performing some straightforward calculations, we reach the relaxation times in branches 1 and 2, and finally obtain the conductivity and the AMR of the system.

- 
- [1] E. I. Rashba, *Sov. Phys. Solid State* **2**, 1109 (1960).  
[2] F. T. Vas'ko, *JETP Lett.* **30**, 541 (1979).  
[3] Y. A. Bychkov and E. I. Rashba, *JETP Lett.* **39**, 78 (1984).  
[4] P. Sharma, *Science* **307**, 531 (2005).  
[5] I. Zutić, J. Fabian, and S. Das Sarma, *Rev. Mod. Phys.* **76**, 323 (2004).  
[6] M. Alidoust and K. Halterman, *New J. Phys.* **17**, 033001 (2015).  
[7] M. Alidoust and K. Halterman, *J. Phys.: Condens. Matter* **27**, 235301 (2015).  
[8] E. Cappelluti, C. Grimaldi, and F. Marsiglio, *Phys. Rev. Lett.* **98**, 167002 (2007).  
[9] C. Grimaldi, *Phys. Rev. B* **72**, 075307 (2005).  
[10] L. Wu, J. Yang, S. Wang, P. Wei, J. Yang, W. Zhang, and L. Chen, *Appl. Phys. Lett.* **105**, 202115 (2014).  
[11] C. Xiao, D. Li, and Z. Ma, *Phys. Rev. B* **93**, 075150 (2016).  
[12] T. S. Nunner, G. Zaránd, and F. von Oppen, *Phys. Rev. Lett.* **100**, 236602 (2008).  
[13] R. Žitko and J. Bonča, *Phys. Rev. B* **84**, 193411 (2011).  
[14] M. Zarea, S. E. Ulloa, and N. Sandler, *Phys. Rev. Lett.* **108**, 046601 (2012).  
[15] L. Isaev, D. F. Agterberg, and I. Vekhter, *Phys. Rev. B* **85**, 081107(R) (2012).  
[16] Z. B. Yan, X. S. Yang, L. Sun, and S. L. Wan, *Eur. Phys. J. B* **85**, 417 (2012).  
[17] K. Vyborný, A. A. Kovalev, J. Sinova, and T. Jungwirth, *Phys. Rev. B* **79**, 045427 (2009).  
[18] J. D. Walls, J. Huang, R. M. Westervelt, and E. J. Heller, *Phys. Rev. B* **73**, 035325 (2006).  
[19] K. Akabli, Y. Magnin, M. Oko, I. Harada, and H. T. Diep, *Phys. Rev. B* **84**, 024428 (2011).  
[20] K. Akabli and H. T. Diep, *Phys. Rev. B* **77**, 165433 (2008).  
[21] A. N. Zarezad and J. Abouie, *Phys. Rev. B* **98**, 155413 (2018).  
[22] C. R. Ast, J. Henk, A. Ernst, L. Moreschini, M. C. Falub, D. Pacilé, P. Bruno, K. Kern, and M. Grioni, *Phys. Rev. Lett.* **98**, 186807 (2007).  
[23] C. R. Ast, D. Pacilé, L. Moreschini, M. C. Falub, M. Papagno, K. Kern, M. Grioni, J. Henk, A. Ernst, S. Ostanin, and P. Bruno, *Phys. Rev. B* **77**, 081407(R) (2008).  
[24] L. Moreschini, A. Bendounan, H. Bentmann, M. Assig, K. Kern, F. Reinert, J. Henk, C. R. Ast, and M. Grioni, *Phys. Rev. B* **80**, 035438 (2009).  
[25] I. Gierz, T. Suzuki, E. Frantzeskakis, S. Pons, S. Ostanin, A. Ernst, J. Henk, M. Grioni, K. Kern, and C. R. Ast, *Phys. Rev. Lett.* **103**, 046803 (2009).  
[26] K. Ishizaka, M. Bahramy, H. Murakawa, M. Sakano, T. Shimojima, T. Sonobe, K. Koizumi, S. Shin, H. Miyahara, A. Kimura *et al.* *Nat. Mater.* **10**, 521 (2011).  
[27] S. V. Eremeev, I. A. Nechaev, Y. M. Koroteev, P. M. Echenique, and E. V. Chulkov, *Phys. Rev. Lett.* **108**, 246802 (2012).

- [28] S. V. Eremeev, I. P. Rusinov, I. A. Nechaev, and E. V. Chulkov, *New J. Phys.* **15**, 075015 (2013).
- [29] G. Landolt, S. V. Eremeev, Y. M. Koroteev, B. Slomski, S. Muff, T. Neupert, M. Kobayashi, V. N. Strocov, T. Schmitt, Z. S. Aliev, M. B. Babanly, I. R. Amiraslanov, E. V. Chulkov, J. Osterwalder, and J. H. Dil, *Phys. Rev. Lett.* **109**, 116403 (2012).
- [30] G. Landolt, S. V. Eremeev, O. E. Tereshchenko, S. Muff, B. Slomski, K. A. Kokh, M. Kobayashi, T. Schmitt, V. N. Strocov, J. Osterwalder, E. V. Chulkov, and J. H. Dil, *New J. Phys.* **15**, 085022 (2013).
- [31] A. Crepaldi, L. Moreschini, G. Autès, C. Tournier-Colletta, S. Moser, N. Virk, H. Berger, P. Bugnon, Y. J. Chang, K. Kern, A. Bostwick, E. Rotenberg, O. V. Yazyev, and M. Grioni, *Phys. Rev. Lett.* **109**, 096803 (2012).
- [32] A. Manchon and S. Zhang, *Phys. Rev. B* **78**, 212405 (2008).
- [33] P. Liu and S.-J. Xiong, *Eur. Phys. J. B* **51**, 513 (2006).
- [34] J. K. Furdyna and J. Kossut, *Semiconductors and Semimetals*, Vol. 25 (Academic Press, London, 1988).
- [35] J. Schliemann and D. Loss, *Phys. Rev. B* **68**, 165311 (2003).
- [36] M. Trushin, K. Výborný, P. Moraczewski, A. A. Kovalev, J. Schliemann, and T. Jungwirth, *Phys. Rev. B* **80**, 134405 (2009).
- [37] C. Xiao, D. Li, and Z. Ma, *Front. Phys.* **11**, 117201 (2016).
- [38] Y. Fukuma, H. Asada, N. Nishimura, and T. Koyanagi, *J. Appl. Phys.* **93**, 4034 (2003).
- [39] S. Schulz, I. A. Nechaev, M. Güttler, G. Poelchen, A. Generalov, S. Danzenbächer, A. Chikina, S. Seiro, K. Kliemt, A. Yu. Vyazovskaya, T. K. Kim, P. Dudin, E. V. Chulkov, C. Laubschat, E. E. Krasovskii, C. Geibel, C. Krellner, K. Kummer, and D. V. Vyalikh, *npj Quantum Mater.* **4**, 26 (2019).
- [40] A. Sabzalipour, J. Abouie, and S. H. Abedinpour, *J. Phys.: Condens. Matter.* **27**, 115301 (2015).
- [41] N. A. Sinitsyn, *J. Phys.: Condens. Matter* **20**, 023201 (2008).
- [42] Y. Tokura, *Phys. Rev. B* **58**, 7151 (1998).